Title	Cocrystal forms of the BCS class IV drug sulfamethoxazole
Author(s)	Alsubaie, Moneerh; Aljohani, Marwah; Erxleben, Andrea; McArdle, Patrick
Publication Date	2018-05-23
Publication Information	Alsubaie, Moneerh, Aljohani, Marwah, Erxleben, Andrea, & McArdle, Patrick. (2018). Cocrystal Forms of the BCS Class IV Drug Sulfamethoxazole. Crystal Growth & Design, 18(7), 3902-3912. doi: 10.1021/acs.cgd.8b00216
Publisher	American Chemical Society
Link to publisher's version	https://dx.doi.org/10.1021/acs.cgd.8b00216
Item record	http://hdl.handle.net/10379/14819
DOI	http://dx.doi.org/10.1021/acs.cgd.8b00216

Co-crystal forms of the BCS class IV drug sulfamethoxazole

Moneerh Alsubaie, Marwah Aljohani, Andrea Erxleben* and Patrick McArdle*

School of Chemistry, National University of Ireland, Galway, Ireland

*Corresponding author email address: andrea.erxleben@nuigalway.ie (AE);
p.mcardle@nuigalway.ie (PM)

Abstract

Sulfamethoxazole, smz, is an antibiotic which is classified as a Biopharmaceutics Classification System (BCS) class IV, low solubility and low permeability drug. Co-crystal formation has been examined in an attempt to improve solubility. Both ball milling and crystallization from solution have been examined. Ball milling showed that thirteen co-formers gave new crystalline X-ray powder patterns and four gave X-ray amorphous patterns while crystallization from solution gave single crystals of four co-crystals and a salt. The co-formers which gave the co-crystals and the salt have better H-bond acceptors than the sulfonyl oxygens of smz. The 4,4-dipyridyl co-crystal has an interesting high Z'' structure. It crystallized in space group P1 with four smz and six 4,4'-dipyridyl molecules in the asymmetric unit. The highest dissolution rate among the smz co-crystal and co-amorphous systems was shown by the 1,3-di(4-pyridyl)propane co-crystal.

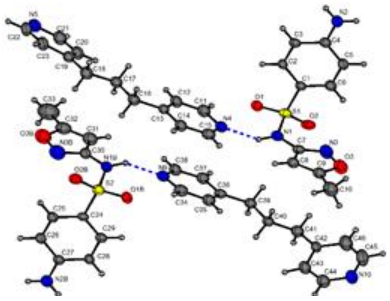

Co-crystal forms of the BCS class IV drug sulfamethoxazole

Moneerh Alsubaie, Marwah Aljohani, Andrea Erxleben* and Patrick McArdle*

School of Chemistry, National University of Ireland, Galway, Ireland

*Corresponding author email address: andrea.erxleben@nuigalway.ie (AE);
p.mcardle@nuigalway.ie (PM)

Abstract

Sulfamethoxazole, smz, is an antibiotic which is classified as a Biopharmaceutics Classification System (BCS) class IV, low solubility and low permeability drug. Co-crystal formation has been examined in an attempt to improve solubility. Both ball milling and crystallization from solution have been examined. Ball milling showed that thirteen co-formers gave new crystalline X-ray powder patterns and four gave X-ray amorphous patterns while crystallization from solution gave single crystals of four co-crystals and a salt. The co-formers which gave the co-crystals and the salt have better H-bond acceptors than the sulfonyl oxygens of smz. The 4,4-dipyridyl co-crystal has an interesting high Z'' structure. It crystallized in space group P1 with four smz and six 4,4'-dipyridyl molecules in the asymmetric unit. The highest dissolution rate among the smz co-crystal and co-amorphous systems was shown by the 1,3-di(4-pyridyl)propane co-crystal.

1. Introduction

Sulfamethoxazole, smz, is an antibiotic which is used to treat urinary tract infections.[1] It is classified in the Biopharmaceutics Classification System (BCS) as a class IV, low solubility and low permeability drug.[2] Co-crystal and co-amorphous formation are established methods for the enhancement of the physical and chemical properties of active pharmaceutical ingredients, APIs. The general problems associated with poorly soluble drugs have been reviewed.[3] Co-crystal formation in particular has been shown to enhance the solubility, dissolution rate and bioavailability of poorly soluble APIs.[4] Studies in our group and elsewhere have demonstrated

that stable co-amorphous forms also improve solubility.[5-8] Co-amorphous systems can be stoichiometric binary systems of two compatible drugs or of a drug and a pharmaceutically acceptable small-molecule co-former.[9, 10]

Four smz polymorphs have been reported, forms I and II have been obtained by solution crystallization at different temperatures[11-13] and forms III and IV have been crystallized from ethyl acetate in the presence of specific polymers.[14] No single crystal or X-ray powder structures of co-crystals or solvates of smz have been reported, however the crystal structure of the trimethoprim salt has been reported. [15] A co-crystal characterized by the appearance of a new X-ray powder diffraction pattern has been reported with L-malic acid.[2] The aim of this work is to understand the factors which control smz co-crystal and co-amorphous formation and to determine their associated relevant physical properties.

2. Experimental Section

2.1 Materials

The active pharmaceutical ingredient sulfamethoxazole, smz, pyrazine, py, *N*-hydroxysuccinimide, hsu, and imidazole, imz, were purchased from TCI Europe. 1,2-di(4-pyridyl)ethylene, ebipy, 1,3-di(4-pyridyl)propane, pbipy, 4.4'-bipyridine, bipy, 4-phenylpyridine, phpy, benzamidine, bza, acetamide, aca, propionamide, ppa, isonicotinamide, ina, 2-hydroxypyridine, hyp, oxalic acid dihydrate, oa, deoxycholic acid, da, sodium deoxycholate, Nada, and hexamethylenetetramine, hma, were from Sigma-Aldrich. Carbamazepine, cbz, was from Alfa Aesar. The polymorphic form of commercial smz was shown by X-ray powder diffraction (XRPD) to be form I. Samples of smz form II were obtained by wrapping 500 mg of commercial smz in aluminium foil and heating it in an oven at 170 °C for 15 mins. After cooling to room temperature XRPD confirmed the presence of form II.

2.2 Methods

2.2.1 Preparation of co-crystals

0.5 g of smz and the respective co-former (1:1 molar ratio) were milled at 25 Hz for 60 min. at room temperature by using an oscillatory ball mill (mixer mill MM400, Retsch GmbH, Haan,

Germany) and a 25 cm^3 stainless steel jar containing one 15 mm diameter stainless steel ball. The milling was stopped for 15 min after 30 min to avoid overheating. XRPD patterns of the products were collected. The powder products were also analysed by infrared (FT-IR) spectroscopy and differential scanning calorimetry (DSC). In attempts to grow single co-crystals from solution smz was dissolved in acetonitrile, methanol or ethanol and a 1 mole equivalent of the respective co-former was dissolved in the same solvent. The solutions were mixed and allowed to evaporate slowly. The smz-bza salt appeared immediately after mixing. The smz.ebipy co-crystal formed after two hours, while the smz.pbipy, smz.bipy and smz.phpy co-crystals formed within one week. The single co-crystals were analysed by single-crystal X-ray diffraction.

2.2.2 Preparation of co-amorphous systems

Co-amorphous smz.cbz and smz.hma were obtained by milling at room temperature, as described above. The mole ratios used were 1:1 for smz.cbz and 1:0.25 for smz.hma. The cryo-milling technique was used to prepare amorphous smz.da and smz.Nada. The milling jar was immersed in liquid nitrogen for 5 min. After milling for 7.5 min. the jar was cooled again in liquid nitrogen for 2.5 min. This process was repeated until milling was completed. The milled products were stored at room temperature in sealed vials. The samples were analysed by XRPD after 1, 7, 14, 30 and 60 days.

2.2.3 Dissolution study

All samples used in the dissolution study were gently ground before use to avoid any bias from large particles. Samples of smz forms I and II, 42.3 mg, and co-crystal and co-amorphous samples containing 42.3 mg of smz were placed in 900 mL of 0.1 M phosphate buffer (pH 5.5, 37 °C), stirred at 50 rpm using a VanKel E7149 dissolution apparatus. 2.5 mL aliquots were withdrawn at predetermined times (2, 5, 10, 15, 25, 30, 45, 60, 90, 120, and 180 min.) and immediately replaced with 2.5 mL of the dissolution medium. The samples were analysed immediately using UV/Vis spectroscopy (Varian Cary 50 Scan Spectrophotometer using quartz cuvettes at 255 nm). All dissolution experiments were performed in duplicate. Standard solutions of smz were prepared in phosphate buffer (0.1 M, pH 5.5). The resulting calibration curve was linear in the relevant concentration range. Overlapping absorbances were treated by measurements at two suitable wavelengths and simultaneous analysis.[17] The

wavelengths used were smz.ebipy 255 and 270, smz.pbipy 255 and 270, smz.bipy 255 and 240, smz.phpy 255 and 300 and $bza^{+}smz^{-}$ 255 and 228 nm.

The solubilities of smz forms I and II, the co-formers and the co-crystals in phosphate buffer were measured at 37 °C.[18] The solubilities of the co-formers in mg mL^{-1} and their ratios to that of smz form I, in parenthesis, were found to be smz form I 0.705, smz form II 1.447, ebipy 1.606(2.3), pbipy 15.019(21.3), bipy 4.435(6.3), phpy 1.057(1.5).

2.2.4 X-ray powder diffraction

X-ray powder patterns were recorded on an Inel Equinox 3000 powder diffractometer between 5 and 90 ° (2θ) using Cu K_α radiation (λ = 1.54178 Å, 35 kV, 25 mA).

2.2.5 Single crystal X-ray diffraction

An Oxford Diffraction Xcalibur system was used to collect X-ray diffraction data at room temperature. The crystal structures were solved using ShelxT and refined using ShelxL 2016/6 within the Oscail package.[19-21] CIF files can be obtained free of charge at www.ccdc.cam.ac.uk/conts/retrieving.html or from the Cambridge Crystallographic Data Centre, Cambridge, UK with the REF codes 1822377 (smz.ebipy), 1822378 (smz.pbipy), 1822379 (smz.bipy), 1822380 (smz.phpy), 822381 (smz.bza), 822382 (smz.0.5H2O)).

2.2.6 Molecular orbital calculations

Molecular orbital calculations were carried out using Gaussian 09. [22] The DFT calculations used the B3LYP functional and 6-31G* basis sets. Atom coordinates for smz were taken from CSD code Slfnmb07, optimized and the gas phase IR spectrum was calculated. An anharmonicity correction of 0.96 was applied to the calculated vibrational frequencies. The atom charges listed in Figures S1 and S2 are Mulliken charges. The energy profile shown in Figure 12 and the structure of smz.0.25hma was calculated using the Mopac AM1 method.

2.2.7 IR spectroscopy

FT-IR spectra were recorded on a Perkin Elmer Spectrum 400 fitted with an ATR reflectance attachment. Spectra were collected in the 650 − 3600 cm^{-1} range with a resolution of 4 cm^{-1} and four integrated scans using diamond/ZnSe optics.

2.2.8 Differential scanning calorimetry

A STA625 thermal analyser from Rheometric Scientific (Piscataway, New Jersey) was used to perform thermal analysis. The heating rate was 10 °C/min and the runs were performed between 20 °C and 300 °C. Open aluminium crucibles were used, nitrogen was purged in the ambient mode and an indium standard was used for calibration.

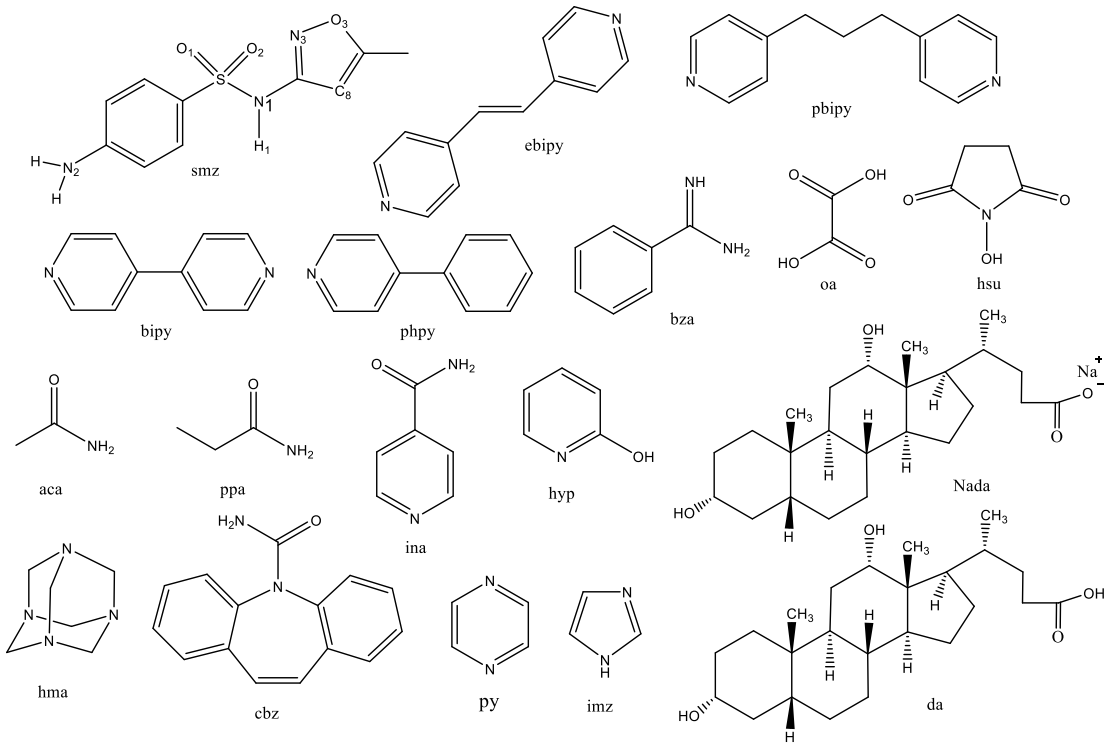

Scheme 1.

3. Results and discussion

3.1 Co-crystal screen

A motif search of the CSD using X-NH-SO2-X and a general pyridine co-former gave thirty nine potential candidates. The compatibility of smz and the potential co-formers was tested using the multi-component screening, Molecular Complementarity, function in the Mercury program.[23]

This prediction and the observed results are presented in Table S1. The co-formers were then examined by ball milling smz and the co-former. The co-formers which gave new XRPD patterns are listed in Table 1 and illustrated in Scheme 1. The co-formers that gave stable co-amorphous systems and those for which single crystals could be obtained are also indicated in Table 1. 1:1 mole ratios were used in initial experiments and if no or incomplete changes were observed in the XRPD patterns other ratios were used. For example in the case of hma a strong hma XRPD peak was observed when the smz:hma ratio was 1:1. The hma peak disappeared when the ratio was 1:0.25. The potential co-formers which gave simple physical mixtures and the solvents used for the solution crystallization experiments are listed in the supporting information, Tables S2, S3. It has been reported that L-malic acid gave a co-crystal using the gas anti solvent method and by slow evaporation of acetone solutions.[2] Milling smz and L-malic acid in a 1:1 mole ratio did not show any new X-ray diffraction peaks. Addition of a few drops of acetonitrile and ethanol to the milling jar did not alter the results.

3.2 IR spectra and hydrogen bonding

The IR and Raman spectra of smz forms I and II and the hemi hydrate have been analysed using deuteration studies, expected hydrogen bonding frequency shifts and the strength of the hydrogen bonding as monitored by the observed D…A distances.[24] In the present work the shifts observed between the calculated gas phase IR spectrum of smz and the FT-IR spectra of the hydrogen bonded solids are compared to observed D…A distances, the latter being a measure of hydrogen bond strength. The N-H and C8-H8 vibrational frequencies calculated were, $-NH_2$ ν(as) 3674, $-NH_2$ ν(s) 3573, ν(N1-H1) 3537 and ν(C8-H8) 3306 cm^{-1}. The corresponding observed IR frequencies from smz form I, with shifts from the gas phase frequencies in parenthesis were 3466(208), 3376(197), 3297(240) and 3144(162) cm^{-1} respectively. The corresponding D…A distances (taken from CSD entry SLFNMB07) were 3.287, 3.318, 3.246 and 3.237 Å. It is noticeable that all of the smz D…A distances are greater than 3.2 Å indicating that the hydrogen bonds in smz form I are relatively weak. The IR peak assignment given here is in agreement with the earlier work.[24] The FT-IR for smz and the co-crystals are in the supporting information. Where it was possible the N-H stretching frequencies and their shifts from the values calculated for gas phase smz are assigned in the hydrogen bonding table, Table 3. It is noticeable that the observed IR frequency shifts for the co-crystals are larger than the 240 – 162 cm^{-1} range observed for smz form I indicating stronger hydrogen bonding in the co-crystals. The IR spectra of the 1:1 and 1:0.5

smz.ebipy co-crystals had almost identical IR spectra for the N-H vibrations suggesting that both smz molecules in the latter have similar hydrogen bonding.

3.3 H-bonding in smz polymorphs

The crystal structures of the four smz polymorphs have been reported however there has been no analysis of their hydrogen bonding differences. Since co-crystal formation will inevitably involve a replacement or a major alteration of existing smz hydrogen bonding both smz and co-crystal H-bonding are discussed here. The crystal structure of the hemi-hydrate has been repeated as the coordinates of the previous determination have not been deposited on the CSD.[24] The X-ray data for four co-crystals, the bza salt and the hemi-hydrate are in Table 2. Hydrogen bonding is to a considerable extent electrostatic in nature and the relative importance of H-bond donors and acceptors are reflected in calculated atom charges. A DFT calculation has been used to obtain atom charges for smz (Fig. S1). The suggested order of H-bond donors and acceptors is N1-H > N2-H and N1 > O1, O2 > N2 > O3 > N3. However, N1 does not have a sterically active lone pair and O1 and O2 are the strongest effective H-bond acceptors. In the smz form I structure there are three H-bonding interactions. The strongest is N1-H…O2, D…A 3.246(3) Å, followed by N2-H…O1, D…A 3.287(3) Å, and N2-H…O1, D…A 3.318(3) Å, which form fused $R_4^3(18)$ and $R_3^3(10)$ rings, using graph sets described by Etter,[25] which combine to generate sheets which are stacked in an interdigitated fashion along the *c* axis (Fig. 1).

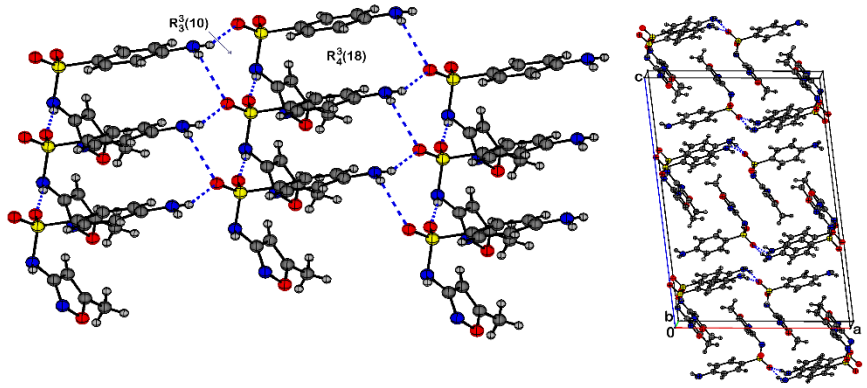

Figure 1. H-bonding and unit cell packing in smz form I.

In smz form II the strongest H-bond donor, N1, interacts with the weakest H-bond acceptor N3, however this interaction results in stable $R_2^2(8)$ ring formation. N2-H…O1 and N2-H…O2 hydrogen bonds form $R_4^4(22)$ rings which combine to give sheets which are connected in pairs by the $R_2^2(8)$ rings. These double sheets are then stacked along the *a* axis (Fig. 2).

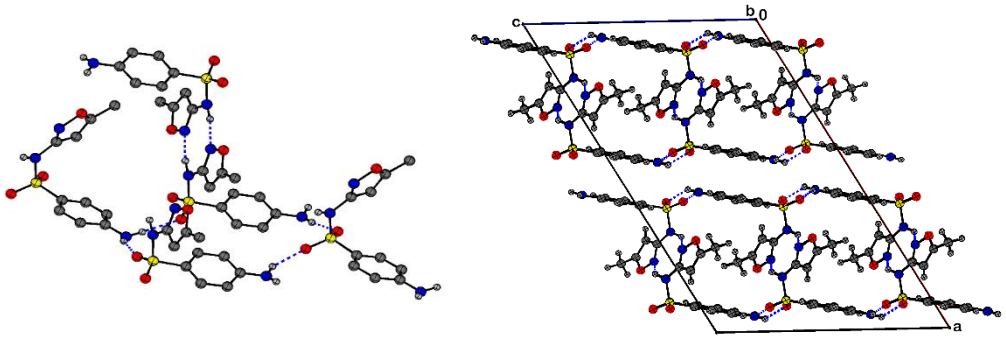

Figure 2. H-bonding and unit cell packing in smz form II.

Smz form III has a H-bonding network that is closely related to that of form II. Again $R_4^4(22)$ rings form sheets which are connected in pairs by $R_2^2(8)$ rings but here there is one double sheet per unit cell (Fig. 3).

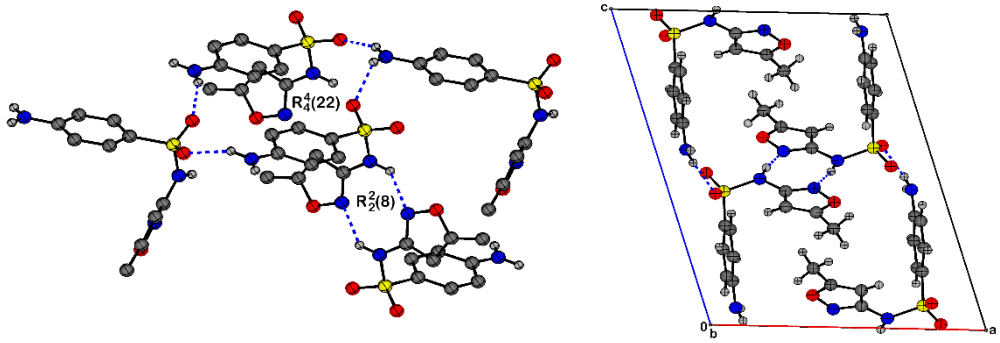

Figure 3. H-bonding and unit cell packing in smz form III.

In smz form IV the strongest donor forms a H-bond to the strongest acceptor (N1-H1…O2, D…A 3.136(2) Å) and the second strongest H-bond donor also forms a H-bond to the strongest acceptor (N2-H4…O1, D…A 3.015(2) Å). The H-bonding network contains $R_3^3(10)$ and $R_3^2(18)$ rings which combine to generate a 3D network, Fig. 4.

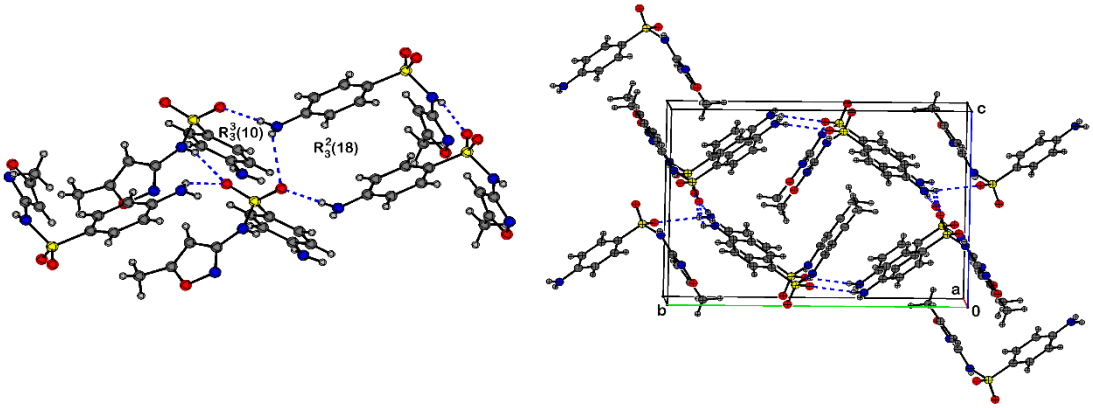

Figure 4. H-bonding and unit cell packing in smz form IV.

3.4 The crystal structure of smz hemihydrate

The crystal structure of smz hemihydrate has been previously reported[24] but its coordinates have not been deposited and its H-bonding analysis was focussed on IR analysis of deuterated derivatives. The asymmetric unit is shown in Fig. 5.

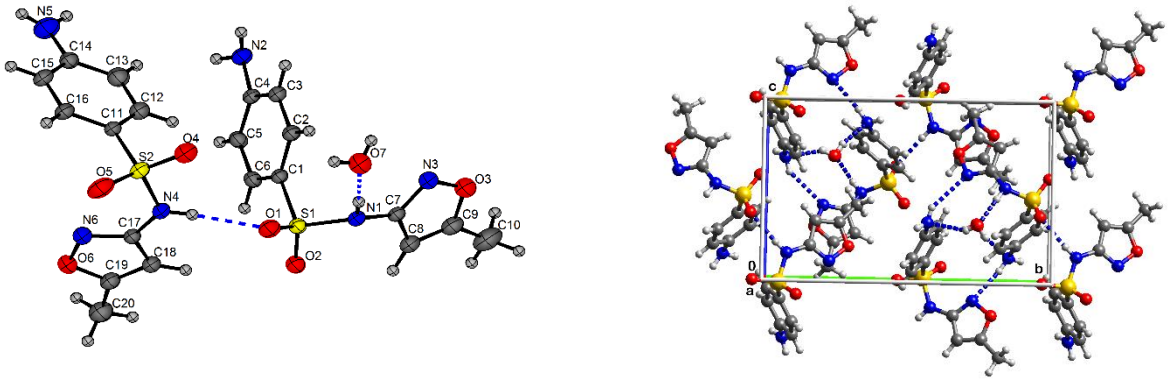

Figure 5. The asymmetric unit and unit cell packing of the smz.0.5H_2O structure.

The strongest smz H-bond donor, the sulphonamide N-H, of one of the smz molecules is H-bonded to the water molecule and the strongest H-bond donor of the second smz molecule is H-bonded to O1 of the first smz molecule, N5-H1…O1, D…A 2.872(4) Å. The second H-bond donor forms a H-bond to the weakest acceptor, N2-H7…N6, D…A 3.072(5) Å. The water molecule forms donor H-bonds to the amino nitrogens of both smz molecules which are in turn H-bonded to sulfur oxygens resulting in a 3D network. All H-bond donors and acceptors except O2 and the ring oxygens are involved in H-bonding.

3.5 The crystal structure of smz.ebipy

The asymmetric unit of smz.ebipy is shown in Fig. 6.

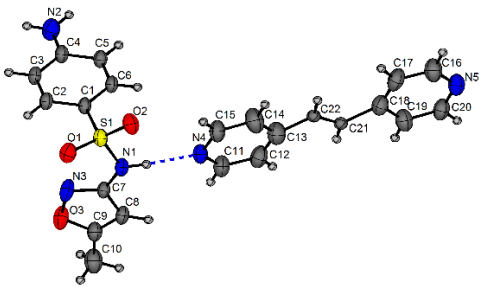

Figure 6. The structure of smz.ebipy (one disorder component only).

Milling experiments indicated that smz and ebipy could form 1:0.5 and 1:1 co-crystals. However only the latter could be grown as a single crystal. In the 1:1 co-crystal the strongest H-bond donor in smz forms a H-bond to ebipy.

Surprisingly only one of the ebipy H-bond acceptors is involved in H-bonding. It is likely that in the 2:1 co-crystal both H-bond acceptors are involved in hydrogen bonding. In the figures the ebipy is reduced to a single N atom for clarity. The H-bonding network contains $R_2^2(20)$ and $R_1^2(6)$ rings which extend to form ladders normal to the *a* axis, Fig. 7. The IR spectrum of smz.ebipy had peaks at 3241(296), 3371(304), 3241(296), 3478(95) and 3135(171) cm^{-1} (with shifts from gas phase calculated smz positions in parenthesis) which are assigned on the basis of the stronger hydrogen bond formed by N1-H1…N4, 2.832(3) Å, Table 3).

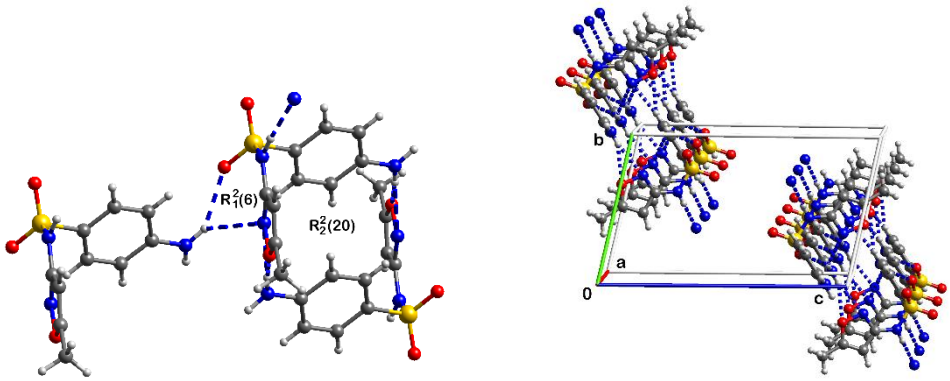

Figure 7. H-bonding and packing of smz.ebipy.

3.6 The crystal structure of smz.pbipy

There are two formula units in the asymmetric unit of the smz.pbipy structure, Fig. 8.

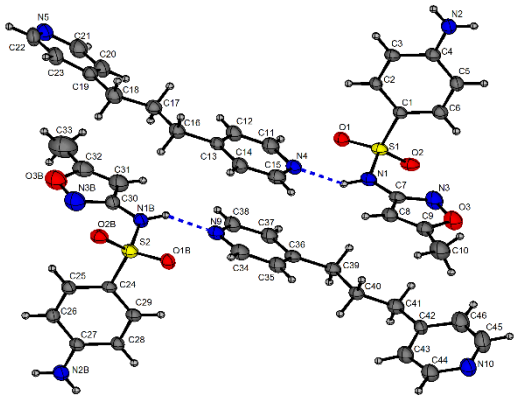

Figure 8. The asymmetric unit of smz.pbipy.

In contrast to the ebipy structure both H-bond acceptors of the pbipy are involved in H-bonding. The two formula units form near identical independent interpenetrating H-bond networks containing $R_6^6(46)$ rings (each formed from four smz.bipy units) which generate independent interpenetrating sheets. One of the large rings is shown in Fig. 9.

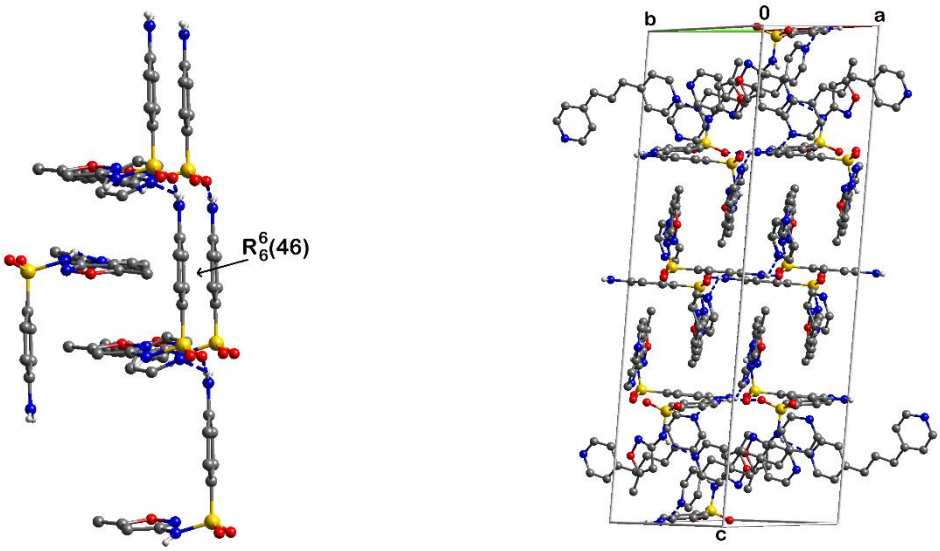

Figure 9. H-bonding and unit cell packing in the smz.pbipy structure.

The sheets are packed in the unit cell such that the pair of layers near the centre of the cell are rotated 90° relative to those nearer the ends of the cell, Fig. 9.

3.7 The crystal structure of smz.bipy

There are four smz and six bipy molecules in the asymmetric unit in space group P1, Fig. 10. The structure therefore has a Z' of 4 and a Z'' of 10.[26] There is an approximate inversion centre at the centre of the unit cell. However, attempts to refine the structure in space group P-1 required extensive disorder modelling and a far more satisfactory result was obtained when the structure was refined in P1. The approximate inversion centre is visible at the centre of the cell and it is reflected in the H-bonding and molecular conformations adopted by the smz molecules.

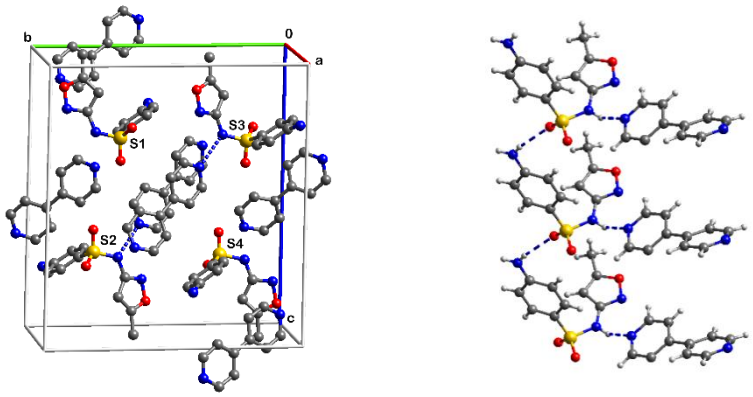

Figure 10. Asymmetric unit and the C(8) chain of the smz.bipy structure.

Each smz forms a relatively strong H-bond from its amide H-bond donor to a bipy which has no H-bond formed by its other H-bond acceptor. Each smz also forms a C(8) chain, Fig. 10. If the sulfur atom numbers are used to label the smz molecules then the remaining two bipys bridge the smzs containing S1 and S2 and S3 and S4 respectively. The conformations of the smz molecules (with the S2 and S4 molecules inverted) are in approximate pairs when superposed, Fig. 11.

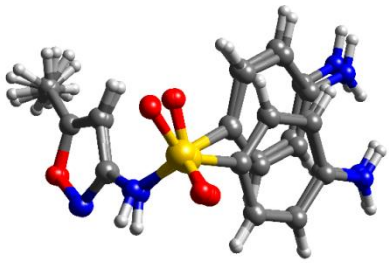

Figure 11. Smz molecules with the atoms of the five membered rings fitted.

There is no such pairing in the conformations of the bipy molecules. Their dihedrals span most of the rotational energy profile, Fig. 12. The minimum bipy torsional energy is at a dihedral angle of 38°. It is therefore within the bipy molecules that the breakdown of symmetry occurs. The balance between internal dihedral angle torsional energy and lattice packing leads to the observed compromise.

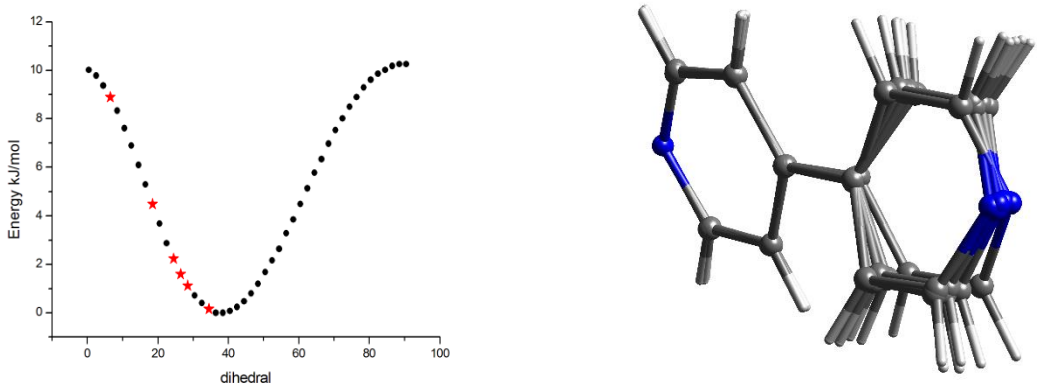

Figure 12. Calculated energy profile for rotation about the ring-ring dihedral (observed values are shown as red stars) and the bipy molecules superposed with one ring fitted.

A previously reported co-crystal formed by cyclopropane carboxylic acid and isonicotinamide had a very high Z' of 12. Interestingly the 12 hydrogen bonded units show a range of pyridine $R_2^2(8)$ ring-ring dihedrals similar to those reported here.[27] The authors suggested that the structure might be an example of a fossil of a solution aggregate persisting in the solid state. Their observation that the structure can also be produced by liquid assisted grinding would seem to make this possibility less likely. In a general review of the factors which appear to influence the adoption of high Z' crystal structures it is suggested that the small rigid nature of the cyclopropane carboxylic acid might be an important factor in the generation of a high Z' structure.[28] The torsion spring/lattice packing balance may be an alternative explanation. Another example of the torsion spring suggestion is bicifidine which switches on heating from the kinetic polymorph, which has one molecule per asymmetric unit, to a polymorph which has four molecules per asymmetric unit with a range of inter ring torsional angles.[29]

3.8 The crystal structure of smz.phpy

Co-crystal formation using the related but simpler phpy co-former was examined to observe an expected simplification of the structure. The asymmetric unit is shown in Fig. 13.

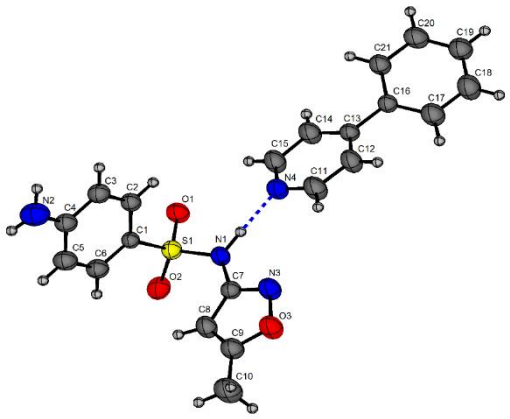

Figure 13. The crystal structure of smz.phpy.

The hydrogen bonding network contains $R_4^4(28)$ rings and C(8) chains which generate a 3D network, Fig. 14. It is clear that just one ring-ring dihedral is adopted in this simpler structure. It is thus likely that the attempt on the part of the co-former in smz.bipy to utilize both of its hydrogen bond acceptors is also an important factor in the generation of the high Z' structure.

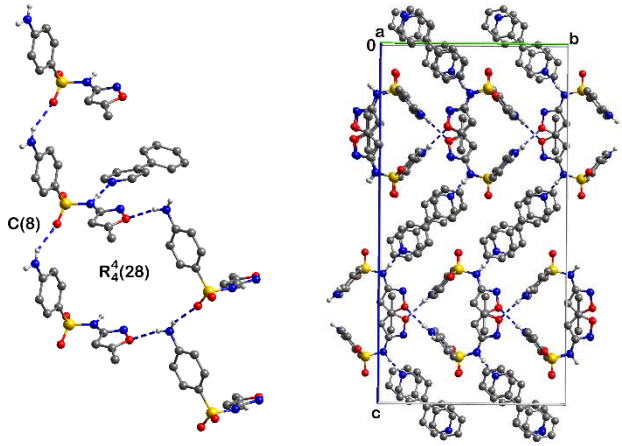

Figure 14. H-bonding and unit cell packing of smz.phpy.

3.9 The crystal structure of smz.bza

The asymmetric unit of smz.bza indicates that salt formation has taken place. The strongest H-bond donor in smz has protonated one of the bza nitrogens and an $R_2^2(8)$ ring is formed, Fig. 15.

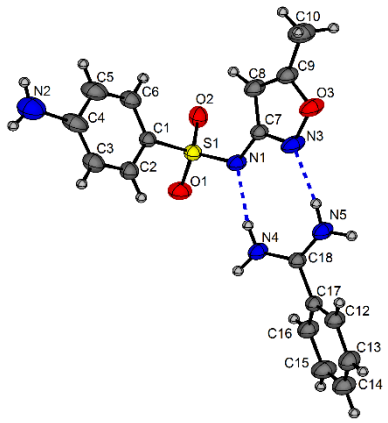

Figure 15. The asymmetric unit of the smz.bza structure.

The H-bonding network contains $R_2^2(8)$ and $R_4^4(12)$ fused rings and extends to give a complex H-bonding network, Fig. 16.

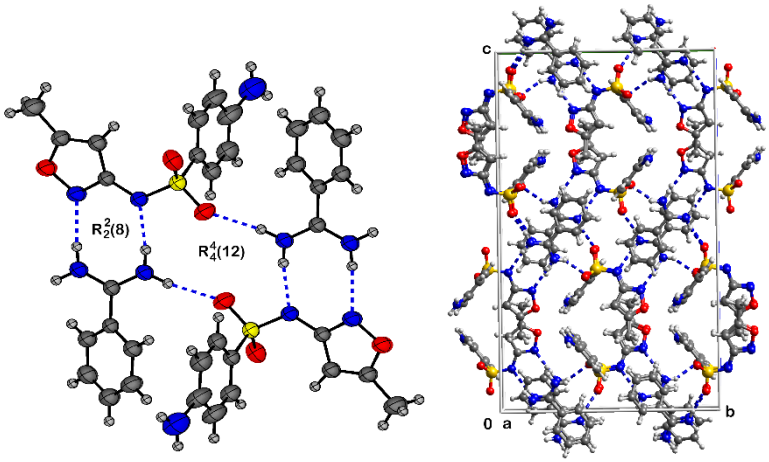

Figure 16. H-bonding and unit cell packing of the smz.bza structure.

In line with literature predictions,[30] calculated atom charges for the cation and the anion indicate that on salt formation the strongest H-bond donor, N1-H, has been converted into the strongest H-bond acceptor and N1 is involved with the strongest H-bond donor of the bza^+ cation in the formation of the $R_2^2(8)$ ring.

3.10 The geometry adopted by smz

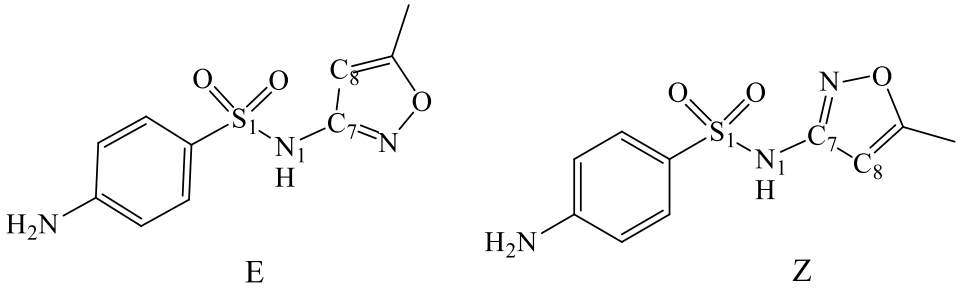

Figure 17. E and Z configurations of smz.

The geometry configuration adopted by twenty four sulphonamides was examined by Perlovich *et al*. [31] and it was concluded that the most important dihedral angle for property analysis, which they labelled τ^3, corresponds to that defined by C8-C7-N1-S1 and the E and Z conformations are shown in Fig. 17. This dihedral is important as it gives an indication of the angle that the rings make with each other and it has the values given in Table 4. The values close to 0 correspond to the E configuration and the values above 160° correspond to the Z configuration. Most of the structures have smz in the E configuration, however the ebipy, pbipy and one of the smz molecules in the hemihydrate have the Z configuration. While it is true that the compound with the largest dihedral has the highest melting point, smz.ebipy, in the other cases no strong correlation is observed between the melting points and the dihedral values, Table 5. A gas phase DFT calculation showed that the E configuration was 12 kJ mol^{-1} more stable than the Z configuration. This difference is small enough to allow crystal packing forces to stabilize the Z configuration in some cases.

3.11 Co-amorphous systems

Neither room temperature milling nor cryo-milling for one hour altered the XRPD pattern of smz. Milling smz with Nada and da at room temperature gave XRPD patterns which were largely amorphous but still had some sharp peaks of the starting compounds. However, cryo milling gave amorphous patterns. These amorphous samples were stable for more than 60 days at 40% relative humidity, RH. Nada and da have been shown to be effective in stabilizing the amorphous

from of a range of APIs.[7] The ability of these two systems to stabilize the amorphous state is probably due to both their H-bonding capabilities and their awkward shape. The latter property makes it difficult for a crystal lattice to grow. When smz was milled with cbz and hma XRPD patterns showed amorphous halos which were stable at 40% RH for one week. These powders crystallized back to the starting materials after two weeks. XRPD patterns are in the supporting information. Milling smz with hma gave results which depended on the smz:hma ratio, Fig. S18. A 1:0.25 mole ratio gave an amorphous halo free of sharp peaks. Other ratios above and below this value had small sharp peaks. At a 1:0.1 mole ratio milling gave samples that were almost completely X-ray amorphous. It is interesting that relatively low amounts of hma which were below any reasonable molecular ratio stabilized the amorphous form. It is also interesting that the relatively small hma molecule can form a 1:0.25 combination with smz which shows some stability. It is highly likely that amorphous smz.0.25hma has formed four N1-H1…N hydrogen bonds at a molecular level. That this is sterically reasonable is demonstrated by the optimized structure shown in Fig. 18. Upon amorphization the largest change in the IR spectrum of smz.hma is seen in the strongest observed peak at 1140 cm^{-1} (calculated position 1132 cm^{-1}). This peak is greatly reduced in intensity and vibrational analysis suggests that the absorption involves symmetric stretching of the SO_2 group. This is most likely due to a change in H-bonding associated with smz hma interaction. It has also been observed that milling of smz alone does not lead to amorphization. This indicates that the co-former is essential for smz amorphization.

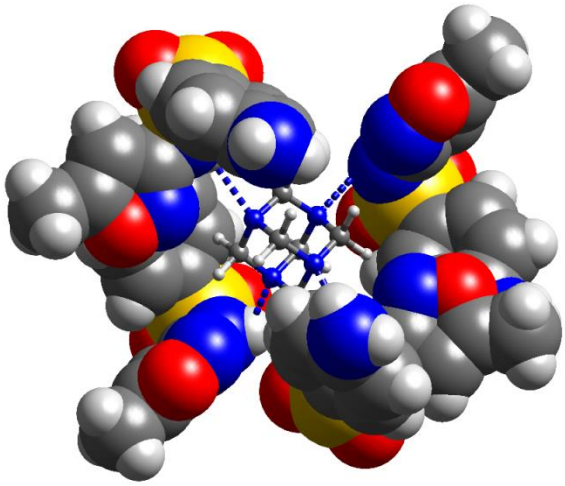

Figure 18. Four smz molecules hydrogen bonded to hma.

3.12 Dissolution study

A dissolution study of smz forms I and II, the ebipy, bipy, phpy, pbipy co-crystals, the co-amorphous systems and the bza salt was carried out at 37 °C in buffer at pH 5.5. The results are shown in Fig. 19. In an attempt to correlate the results with crystal lattice energy an attempt was made to compute lattice energies using the PIXEL program.[32] It was possible to apply the more accurate Pixelc calculation to just two of the co-crystals and the more approximate Clp procedure to all of the structures except the smz.bza salt and smz.ebipy co-crystal which was disordered.[33] The packing indices, PI, and melting points were also examined as these should also be related to lattice energies. It was not possible to calculate a packing coefficient for two of the co-crystals due to disorder in the structures. The results are presented in Table 5.

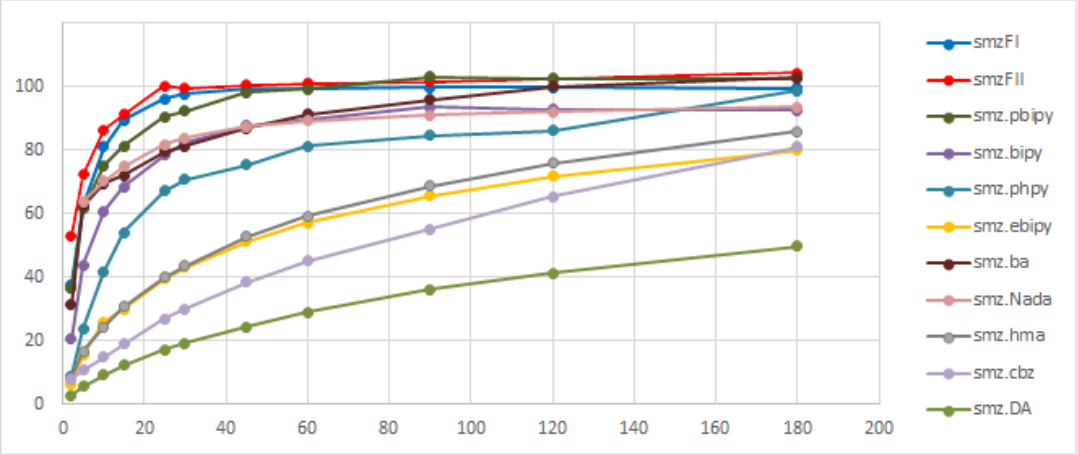

Figure 19. Dissolution rates of smz, smz co-crystals and co-amorphous systems.

The most striking feature of the dissolution study is that after 20 min. smz forms I and II show higher dissolution rates than any of the co-crystals. On the basis that a lower lattice energy should favour dissolution this result is unexpected as smz has a higher lattice energy than any of the co-crystals. There are several recent studies which suggest that co-crystal formation can

enhance API solubility.[34-37] There is also an often quoted rule that API solubility will be enhanced by co-crystal formation if the co-former has more than ten times the solubility of the API.[38-40] This rule is exceeded only in the case of pbipy and within the co-crystals smz.pbipy has indeed got the highest dissolution rate. A recent theoretical study found that there was no clear correlation between lattice energies, calculated dissolution rates and observed dissolution rates.[41] The most reasonable explanation for the higher relative smz dissolution rate is that the process is controlled by the strength of the smz-coformer hydrogen bond. The co-crystals all have a strong hydrogen bond between N1-H1 and the co-former with a D…A distance of approximately 2.8 Å in contrast to the smz structure where all hydrogen bonds have D…A distances > 3.2 Å. The relatively high dissolution rate of smz.pbipy can be reasonably associated with its low Clp energy, low PI and low melting point and high solubility. In contrast, the slow dissolution rate of smz.ebipy is probably due to its high melting point and presumed higher lattice energy. Co-crystals which have higher melting points than their components are relatively rare and have been estimated to be just 14% of all co-crystals.[42] The lack of an enhanced dissolution rate for the smz.bza salt may be due to a high lattice energy indicated by its relatively high melting point. The co-amorphous systems might be expected to have higher dissolution rates than the co-crystals and this is true in the case of Nada. Two of the co-amorphous systems, smz.hma and smz.cbz, recrystallized to starting material in the buffer and smz.da formed a gel on contact with the buffer.[6] Solubility measurements showed that the co-crystals had solubilities that were close to that of smz form I, Table S4. The solubility of smz form II was twice as high as that of smz FI. There was no transformation of metastable smz form II back to stable smz form I during the solubility measurement time (24 hrs.).

4. Conclusions

Four co-crystals of smz have been obtained and their crystal structures determined. The existence of up to nine further potential smz co-crystals is indicated from XRPD and their structures remain to be elucidated. The lattice energies of smz and the co-crystals for which single crystal structures were obtained were estimated using the PIXEL program.

The dissolution rates of the co-crystals are all lower than smz forms I and II despite the fact that they have lower computed lattice energies than smz forms I and II.

It appears that the presence of a stronger hydrogen bond in the co-crystals than those present in smz forms I and II is more important in determining dissolution rates than lattice energies.

Clearly, more studies are needed to fully understand the factors which affect the solubility and dissolution rates of APIs, co-crystals and co-amorphous systems and this will be the focus of future work.

5. Assocciated content

The Supporting Information is available free of charge on the ACS Publications website at DOI:

Atom charges of smz and $bza^{+}smz^{-}$, XRPD patterns of the milling products, statistical prediction of co-crystals formation using the Mercury software, details of the solution crystallization experiments, list of co-formers that did not give co-crystals or co-amorphous systems with smz, solubility data, DSC plots of the co-crystals and salt, IR spectra of the co-crystals and salt.

CCDC 1822377 – 1822382 contain the supplementary crystallographic data for this paper. These data can be obtained free of charge via www.ccdc.cam.ac.uk/data_request/cif, or by emailing data_request@ccdc.cam.ac.uk, or by contacting The Cambridge Crystallographic Data Centre, 12 Union Road, Cambridge CB2 1EZ, UK; fax: +44 1223 336033.

Acknowledgement

This work was supported by Science Foundation Ireland under Grant No. [12/RC/2275] as part of the Synthesis and Solid State Pharmaceutical Centre (SSPC). Moneerh Alsubaie and Marwah Aljohani acknowledge the Saudi Arabian Ministry of Higher Education for Saudi Arabian Government Scholarships.

References

(1) Kesimli, B.; Topacli, A.; Topacli, C. An interaction of caffeine and sulfamethoxazole: studied by IR spectroscopy and PM3 method. *J. Mol. Struct*. **2003**, 645, 199-204 DOI: 10.1016/S0022-2860(02)00561-6

(2) Imchalee, R.; Charoenchaitrakool, M. Gas anti-solvent processing of a new sulfamethoxazole− l-malic acid cocrystal. *J. Ind. Eng. Chem*. **2015**, 25, 12-15 DOI: 10.1016/j.jiec.2014.11.009

(3) Thakuria, R.; Delori, A.; Jones, W.; Lipert, M. P.; Roy, L.; Rodríguez-Hornedo, N. Pharmaceutical cocrystals and poorly soluble drugs. *Int. J. Pharm*. **2013**, 453, 101-125 DOI: 10.1016/j.ijpharm.2012.10.043

(4) Deshpande, P. P.; Singh, J.; Pullockaran, A.; Kissick, T.; Ellsworth, B. A.; Gougoutas, J. Z.; Dimarco, J.; Fakes, M.; Reyes, M.; Lai, C.; Lobinger, H.; Denzel, T.; Ermann, P.; Crispino, G.; Randazzo, M.; Gao, Z.; Randazzo, R.; Lindrud, M.; Rosso, V.; Buono, F.; Doubleday, W. W.; Leung, S.; Richberg, P.; Hughes, D.; Washburn, W. N.; Meng, W.; Volk, K. J.; Mueller, R. H. A Practical Stereoselective Synthesis and Novel Cocrystallizations of an Amphiphatic SGLT-2 Inhibitor. *Org. Process Res. Dev*. **2012**, 16, 577-585 DOI: 10.1021/op200306q

(5) Chieng, N.; Hubert, M.; Saville, D.; Rades, T.; Aaltonen, J. Formation Kinetics and Stability of Carbamazepine−Nicotinamide Cocrystals Prepared by Mechanical Activation. *Cryst. Growth Des*. **2009**, 9, 2377-2386 DOI: 10.1021/cg801253f

(6) Gniado, K.; Löbmann, K.; Rades, T.; Erxleben, A. The influence of co-formers on the dissolution rates of co-amorphous sulfamerazine/excipient systems. *Int. J. Pharm*. **2016**, 504, 20-26 DOI: 10.1016/j.ijpharm.2016.03.023

(7) Gniado, K.; MacFhionnghaile, P.; McArdle, P.; Erxleben, A. The natural bile acid surfactant sodium taurocholate (NaTC) as a coformer in coamorphous systems: Enhanced physical stability and dissolution behavior of coamorphous drug-NaTc systems. *Int. J. Pharm*. **2018**, 535, 132-139 DOI: 10.1016/j.ijpharm.2017.10.049

(8) Suzuki, H.; Ogawa, M.; Hironaka, K.; Ito, K.; Sunada, H. A Nifedipine Coground Mixture with Sodium Deoxycholate. II. Dissolution Characteristics and Stability. *Drug Dev. Ind. Pharm*. **2001**, 27, 951-958 DOI: 10.1081/DDC-100107676

(9) Löbmann, K.; Laitinen, R.; Grohganz, H.; Gordon, K. C.; Strachan, C.; Rades, T. Coamorphous Drug Systems: Enhanced Physical Stability and Dissolution Rate of Indomethacin and Naproxen. *Mol. Pharm*. **2011**, 8, 1919-1928 DOI: 10.1021/mp2002973

(10) Hoppu, P.; Hietala, S.; Schantz, S.; Juppo, A. M. Rheology and molecular mobility of amorphous blends of citric acid and paracetamol. *Eur. J. Pharm. Biopharm*. **2009**, 71, 55-63 DOI: 0939-6411

(11) Luner, P. E.; Majuru, S.; Seyer, J. J.; Kemper, M. S. Quantifying Crystalline Form Composition in Binary Powder Mixtures Using Near-Infrared Reflectance Spectroscopy. *Pharm. Dev. Technol*. **2000**, 5, 231-246 DOI: 10.1081/PDT-100100538

(12) Yang, S. S.; Guillory, J. K. Polymorphism in sulfonamides. *J. pharm. Sci*. **1972**, 61, 26-40 DOI: 10.1002/jps.2600610104

(13) Du, Y.; Xia, Y.; Tang, W.; Hong, Z. *In Characterization of Polymorphism in Sulfamethoxazole Pharmaceutical Molecule Using Terahertz Time-domain Spectroscopy*. International Photonics and Optoelectronics Meetings, Wuhan, 2012/11/01, 2012; Optical Society of America: Wuhan, 2012; p STh4A.07 DOI: 10.1364/LTST.2012.STh4A.07

(14) Price, C. P.; Grzesiak, A. L.; Matzger, A. J. Crystalline Polymorph Selection and Discovery with Polymer Heteronuclei. *J. Am. Chem. Soc*. **2005**, 127, 5512-5517 DOI: 10.1021/ja042561m

(15) Nakai, H.; Takasuka, M.; Shiro, M. X-Ray and infrared spectral studies of the ionic structure of trimethoprim-sulfamethoxazole 1 : 1 molecular complex. *J. Chem. Soc. Perkin Trans*. 2 **1984**, 1459-1464 DOI: 10.1039/P29840001459

(16) Lu, T.; Chen, C. Uncertainty evaluation of humidity sensors calibrated by saturated salt solutions. *Measurement* **2007**, 40, 591-599 DOI: 10.1016/j.measurement.2006.09.012

(17) Sawyer D. T.; Heineman W. R.; J.M., B. *Chemistry Experiments for Instrumental Methods*. ed.; John Wiley & Sons: 1984

(18) Larsson, J. Methods for measurement of solubility and dissolution rate of sparingly soluble drugs. Lund University, 2009.

(19) Sheldrick, G. SHELXT - Integrated space-group and crystal-structure determination. *Acta Crystallogr*. A **2015**, 71, 3-8 DOI: 10.1107/S2053273314026370

(20) Sheldrick, G. M. Crystal structure refinement with SHELXL. *Acta Crystallogr*. C **2015**, 71, 3-8 DOI: 10.1107/S2053229614024218

(21) McArdle, P. Oscail, a program package for small-molecule single-crystal crystallography with crystal morphology prediction and molecular modelling. J. *Appl. Crystallogr*. **2017**, 50, 320 - 326 DOI: 10.1107/S1600576716018446

(22) M. J. Frisch; G. W. Trucks; H. B. Schlegel; G. E. Scuseria; M. A. Robb; J. R. Cheeseman; G. Scalmani; V. Barone; B. Mennucci; G. A. Petersson; H. Nakatsuji; M. Caricato; X. Li; H. P. Hratchian; A. F. Izmaylov; J. Bloino; G. Zheng; J. L. Sonnenberg; M. Hada; M. Ehara; K. Toyota; R. Fukuda; J. Hasegawa; M. Ishida; T. Nakajima; Y. Honda; O. Kitao; H. Nakai; T. Vreven; J. A. Montgomery, J.; J. E. Peralta, F. O.; M. Bearpark; J. J. Heyd; E. Brothers; K. N. Kudin; V. N. Staroverov; R. Kobayashi; J. Normand; K. Raghavachari; A. Rendell; J. C. Burant; S. S. Iyengar; J. Tomasi; M. Cossi; N. Rega; J. M. Millam; M. Klene; J. E. Knox; J. B. Cross; V. Bakken; C. Adamo; J. Jaramillo; R. Gomperts; R. E. Stratmann; O. Yazyev; A. J. Austin; R. Cammi; C. Pomelli; J. W. Ochterski; R. L. Martin; K. Morokuma; V. G. Zakrzewski; G. A. Voth; P. Salvador; J. J. Dannenberg; S. Dapprich; A. D. Daniels; Ö. Farkas; J. B. Foresman; J. V. Ortiz; J. Cioslowski; Fox, D. J. Gaussian 09, Revision B.01. Gaussian, Inc.: Wallingford CT, USA, 2009

(23) Macrae, C. F.; Bruno, I. J.; Chisholm, J. A.; Edgington, P. R.; McCabe, P.; Pidcock, E.; Rodriguez-Monge, L.; Taylor, R.; van de Streek, J.; Wood, P. A. Mercury CSD 2.0 - new features for the visualization and investigation of crystal structures, J. Appl. Crystallogr. 2008, 41, 466-470, DOI: 10.1107/S0021889807067908

(24) Takasuka, M.; Nakai, H. IR and Raman spectral and X-ray structural studies of polymorphic forms of sulfamethoxazole. *Vib. Spectrosc*. **2001**, 25, 197-204 DOI: 10.1016/S0924-2031(01)00089-3

(25) Etter, M. C. Encoding and decoding hydrogen-bond patterns of organic compounds. *Acc. Chem. Res*. **1990**, 23, 120-126 DOI: 10.1021/ar00172a005

(26) van Eijck, B. P.; Kroon J. Structure predictions allowing more than one molecule in the asymmetric unit. *Acta Crystallogr*. B **2000**, 56, 535-542 DOI: 10.1107/S0108768100009721

(27) Lemmerer, A.; Fernandes, M. A. Adventures in co-crystal land: high Z[prime or minute], stoichiometric variations, polymorphism and phase transitions in the co-crystals of four liquid and solid cyclic carboxylic acids with the supramolecular reagent isonicotinamide. *New J. Chem*. **2012**, 36, 2242-2252 DOI: 10.1039/C2NJ40186J

(28) Steed, K. M.; Steed, J. W. Packing Problems: High Z′ Crystal Structures and Their Relationship to Cocrystals, Inclusion Compounds, and Polymorphism. *Chem. Rev*. **2015**, 115, 2895-2933 DOI: 10.1021/cr500564z

(29) McArdle, P.; Gilligan, K.; Cunningham, D.; Dark, R.; Mahon, M. A method for the prediction of the crystal structure of ionic organic compounds - the crystal structures of o-toluidinium chloride and bromide and polymorphism of bicifadine hydrochloride. *CrystEngComm* **2004**, 6, 303-309 DOI: 10.1039/b407861f

(30) Hunter, C. A. Quantifying Intermolecular Interactions: Guidelines for the Molecular Recognition Toolbox. *Angew. Chem. Int.* **2004**, 43, 5310-5324 DOI: 10.1002/anie.200301739

(31) Perlovich, G. L.; Ryzhakov, A. M.; Tkachev, V. V.; Hansen, L. K. Sulfonamide Molecular Crystals: Thermodynamic and Structural Aspects. *Cryst. Growth Des*. **2011**, 11, 1067-1081 DOI: 10.1021/cg1012389

(32) Gavezzotti, A. Calculation of lattice energies of organic crystals: the PIXEL integration method in comparison with more traditional methods. *Z. Krist-Cryst. Mater*. **2005**, 220, 499-510 DOI: 10.1524/zkri.220.5.499.65063

(33) Gavezzotti, A.; Colombo, V.; Lo Presti, L. Facts and Factors in the Formation and Stability of Binary Crystals. *Cryst. Growth Des*. **2016**, 16, 6095-6104 DOI: 10.1021/acs.cgd.6b01146

(34) Arafa, M. F.; El-Gizawy, S. A.; Osman, M. A.; El Maghraby, G. M. Co-crystallization for enhanced dissolution rate of nateglinide: In vitro and in vivo evaluation. *J. Drug Deliv. Sci. Tec*. **2017**, 38, 9-17 DOI: 10.1016/j.jddst.2017.01.005

(35) Cherukuvada, S.; Babu, N. J.; Nangia, A. Nitrofurantoin–p-aminobenzoic acid cocrystal: Hydration stability and dissolution rate studies. *J. Pharm. Sci*. **2011**, 100, 3233-3244 DOI: 10.1002/jps.22546

(36) Goud, N. R.; Gangavaram, S.; Suresh, K.; Pal, S.; Manjunatha, S. G.; Nambiar, S.; Nangia, A. Novel Furosemide Cocrystals and Selection of High Solubility Drug Forms. *J. Pharm. Sci*. **2012**, 101, 664-680 DOI: 10.1002/jps.22805

(37) Sanphui, P.; Tothadi, S.; Ganguly, S.; Desiraju, G. R. Salt and Cocrystals of Sildenafil with Dicarboxylic Acids: Solubility and Pharmacokinetic Advantage of the Glutarate Salt. *Mol. Pharm*. **2013**, 10, 4687-4697 DOI: 10.1021/mp400516b

(38) Bolla, G.; Sanphui, P.; Nangia, A. Solubility advantage of tenoxicam phenolic cocrystals compared to salts. *Cryst. Growth Des*. **2013**, 13, 1988-2003 DOI: 10.1021/cg4000457

(39) Alhalaweh, A.; Roy, L.; Rodríguez-Hornedo, N.; Velaga, S. P. pH-dependent solubility of indomethacin–saccharin and carbamazepine–saccharin cocrystals in aqueous media. *Mol. Pharm*. **2012**, 9, 2605-2612 DOI: 10.1021/mp300189b

(40) Elder, D. P.; Holm, R.; de Diego, H. L. Use of pharmaceutical salts and cocrystals to address the issue of poor solubility. *Int. J. Pharm*. **2013**, 453, 88-100 DOI: 10.1016/j.ijpharm.2012.11.028

(41) Liljeblad, A. Evaluation of crystalline solid properties, Experimental and theoretical comparison of polymorphs, solvates and co-crystals. Chalmers University of Technology, Gothenburg, 2015

(42) Perlovich, G. L. Two-component molecular crystals: evaluation of the formation thermodynamics based on melting points and sublimation data. *CrystEngComm* **2017**, 19, 2870-2883 DOI: 10.1039/C7CE00554G

Table 1. Co-crystals and co-amorphous systems of smz obtained by milling.

Co-former	Molar ratio	Result
acetamide, aca	1:1	co-crystal
propionamide, ppa	1:1	co-crystal
isonicotinamide, ina	1:1	co-crystal
2-hydroxypyridine, hyp	1:1	co-crystal
pyrazine, py	1:1	co-crystal
imidazole, imz	1:1	co-crystal
oxalic acid dihydrate, oa	1:1	co-crystal
N-hydroxysuccinimide, hsu	1:1	co-crystal
1,2-di(4-pyridyl)ethylene, ebipy	1:0.5	co-crystal
1,2-di(4-pyridyl)ethylene, ebipy	1:1	co-crystal*
1,3-di(4-pyridyl)propane, pbipy	1:1	co-crystal*
4,4'-bipyridine, bipy	2:3	co-crystal*
4-phenylpyridine, phpy	1:1	co-crystal*
benzamidine, bza	1:1	salt*
carbamazepine, cbz	1:1	co-amorphous
hexamethylenetetramine, hma	1:0.25	co-amorphous
deoxycholic acid, da,	1:1	co-amorphous
sodium deoxycholate, Nada	1:1	co-amorphous

*single crystal grown from solution

Table 2. Crystal data.

	smz.ebipy	smz.pbipy	smz.bipy	smz.phpy	smz.bza	smz.0.5H_2O
Formula	$C_{22}H_{21}N_5O_3S$	$C_{23}H_{25}N_5O_3S$	$C_{25}H_{23}N_6O_3S$	$C_{21}H_{20}N_4O_3S$	$C_{17}H_{19}N_5O_3S$	$C_{10}H_{12}N_3O_{3.5}S$
M_r	435.50	451.54	325.04	408.47	373.43	262.29
Crystal colour and habit	yellow block	colourless block	colourless block	colourless block	colourless block	colourless block
Crystal size (mm)	0.50 x 0.40 x 0.20	0.50 x 0.40 x 0.20	0.50 x 0.40 x 0.20	0.50 x 0.40 x 0.20	0.50 x 0.40 x 0.20	0.50 x 0.40 x 0.20
Crystal system	Triclinic	Monoclinic	Triclinic	Orthorhombic	Orthorhombic	Monoclinic
Space group	P-1	$P2_1/n$	P1	Pbcn	Pbcn	$P2_1$
Unit cell dimensions						
a [Å]	8.2398(6)	16.545(3)	8.2995(3)	8.1529(5)	8.1807(5)	8.3539(3)
b [Å]	9.4266(6)	8.4713(9)	16.4425(7)	16.2187(13)	16.5118(10)	15.0979(6)
c [Å]	15.1888(10)	33.342(5)	17.8000(9)	31.1239(19)	27.3331(17)	9.7151(4)
α [°]	75.792(5)	90	87.800(4)	90	90	90
β [°]	75.151(6)	101.508(19)	78.938(4)	90	90	101.650(4)
γ [°]	72.050(6)	90	88.929(3)	90	90	90
V[$Å^3$]	1066.94(13)	4579.1(12)	2382.02(18)	4115.5(5)	3692.1(4)	1200.09(8)
Z	2	8	4	8	8	4

D_{calc} (g cm^{-3})	1.356	1.310	1.360	1.318	1.344	1.452
No. measd. reflections	8192	19414	19310	12444	10324	5359
No. unique. reflections	4919	10646	13192	4815	4261	4435
No. obs. reflections	3445	2637	8994	1936	2721	3860
Final R1,wR2(obs. refl)	0.0567, 0.1339	0.0924, 0.1919	0.0505, 0.1118	0.0580, 0.1028	0.0599, 0.1534	0.0356, 0.0825
Goodness-of-fit (obs. refl)	1.032	0.896	1.006	0.934	0.903	0.971

Table 3. Hydrogen bonding and IR data.

D-H···A	d(D···A) (Å)	∠(DHA) (°)	symmetry code	IR/cm^{-1} (shift relative to gas phase)
smz.ebipy				
N1-H1...N4	2.832(3)	174(3)	x,y,z	3371(304)
N2-H4...O1	3.096(4)	147(3)	x+1,y,z	3241(296)
N2-H7...O3	3.211(3)	157(3)	-x+1,-y+2,-z	3478(95)
N2-H7...N3	3.247(3)	168(3)	-x+1,-y+2,-z	
smz.pbipy				
N1-H1...N4	2.826(7)	143.1	x,y,z	3195(343)
N1B-H1B...N9	2.824(7)	141.7	x,y,z	
N2-H4...N5	3.096(9)	145.0	x+1,y,z	3461, 3430, 3403, 3322
N2-H7...O2	3.030(6)	167	x,y-1,z	
N2B-H7B...N10	3.092(8)	141.5	x-1,y,z	
N2B-H4B...O2B	3.053(6)	167.0	x,y+1,z	
smz.bipy				
N2-H1N2...N13	2.754(7)	144.9	x,y,z	3190(347)
N5-H1N5...N19	2.769(7)	146.1	x,y,z	
N8-H1N8...N18	2.742(7)	149.2	x,y,z	
N11-H11...N23	2.751(7)	146.6	x,y,z	
N1-H1A...O2	3.052(6)	154.7	x-1,y,z	3452, 3313
N4-H4A...O4	3.084(6)	158.9	x-1,y,z	
N7-H7A...O8	3.094(6)	157.2	x+1,y,z	
N7-H7B...N21	3.077(8)	167.7	x,y,z	
N10-H10E...O10	3.007(6)	153.2	x+1,y,z	
N10-H10F...N22	3.088(8)	172.3	x,y,z	
N1-H1B...N15	3.103(8)	175.7	x,y,z	
N4-H4B...N16	3.121(8)	165.0	x,y,z	

smz.phpy				
N1-H1...N4	2.715(4)	178(3)	x,y,z	3214(323)
N2-H4...O3	3.369(6)	162(3)	x-1/2,y+1/2,-z+1/2	3491(183)
N2-H7...O2	3.089(6)	153(4)	x-1,y,z	3390(183)
C8-H8…O2	3.063(4)	110(3)	x,y,z	3147(162)
smz.bza				
N2-H7A...O2	3.252(15)	140.0	x-1,y,z	3444 - 3227
N2-H4B...N2	2.97(3)	128.1	-x,y,-z+3/2	
N(2A)-H(7A1)...O2	2.899(11)	150.7	x-1,y,z	
N(2A)-H(4A2)...N(2A)	3.08(2)	130.8	-x,y,-z+3/2	
N4-H(1N4)...O1	2.922(3)	172(3)	-x+1,-y+1,-z+1	
N4-H(2N4)...N1	2.910(3)	171(3)	x,y,z	
N5-H(1N5)...N3	2.902(4)	172(3)	x,y,z	
N5-H(2N5)...O2	2.932(3)	149(3)	-x+3/2,y-1/2,z	
smz.0.5H_2O				
N4-H(1N4)...O1	2.872(4)	175(3)	x,y,z	
N1-H(1)...O7	2.757(5)	177(3)	x,y,z	
N5-H(1N5)...O2	3.055(5)	126(5)	x+1,y,z+1	
N5-H(2N5)...N3	3.304(7)	148(5)	-x+1,y+1/2,-z+2	
O7-H(1O7)...N2	2.932(6)	162(5)	x-1,y,z	
O7-H(2O7)...O5	3.015(5)	126(5)	-x,y-1/2,-z+2	
O7-H(2O7)...N5	3.167(7)	147(5)	-x+1,y-1/2,-z+2	
N2-H(4)...O4	2.940(4)	153(3)	x+1,y,z	
N2-H(7)...N6	3.074(5)	167(5)	-x+1,y-1/2,-z+2	

Table 4. Geometry of smz (C8-C7-N1-S dihedral angle) in the smz polymorphs and co-cocrystals.

form/co-crystal		τ^3/°
smz form I		40.82(3)
smz form II		31.98(1)
smz form III		30.37(7)
smz form IV		20.65(2)
smz-ebipy		179.41(2)
		160.91(4)
smz-pbipy		162.69(6)
smz-bipy	S1	3.33(10)
	S2	29.49(10)
	S3	29.66(10)
	S4	1.97(10)
smz-phpy		7.44(5)
		53.36(5)
smz.0.5H_2O		166.28(3)

Table 5. Lattice energy, packing index, melting point and dissolution data of the smz polymorphs and co-crystals.

	Pixelc/kJmol^{-1}	Clp/kJmol^{-1}	% dissolved after 10 min.	PI	Melting point
smz form I	-169.5	-170.4	81	69.6	170.2
smz form II	-165.0	-161.8		68.3	-
smz form III	-171.2	-166.1		67.3	-
smz form IV	-171.9	-167.1		69.2	-
smz.ebipy	-	-	26	-	188.6
smz.pbipy	-	-138.4	75	66.2	128.0
smz.bipy	-	-119.1	61	67.5	167.9
smz.phpy	-129.1	-115.9	42	65.3	122.2
bza^{+}smz^{-}	-	-	70	-	223.9

For Table of Contents Use Only

Co-crystal forms of the BCS class IV drug sulfamethoxazole

Moneerh Alsubaie, Marwah Aljohani, Andrea Erxleben* and Patrick McArdle*

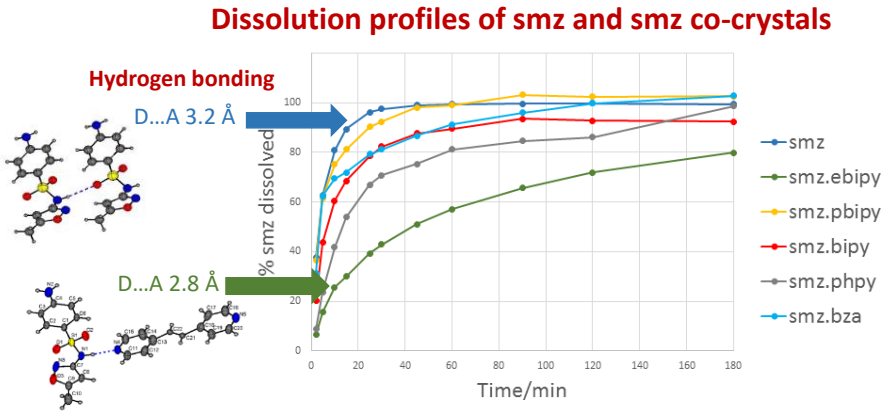

The crystal structures of four co-crystals and a salt of sulfamethoxazole were determined. The dissolution rates of the co-crystals are all lower than those of the sulfamethoxazole polymorphs smz form I and form II despite the fact that they have lower computed lattice energies.